Sensors & Actuators: B. Chemical 418 (2024) 136284

Contents lists available at ScienceDirect

Sensors and Actuators: B. Chemical

journal homepage: www.elsevier.com/locate/snb

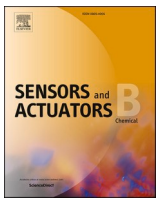

Lighting and rapid detection of the Coronavirus S protein using computationally speculated ligand and its application in SARS-CoV-2

Yuan Liu [a,1], Xiaoyu Xie [b,1], Qingyuan Wang [a,1], Desheng Chen [c,*], Dehui Qiu [c], Xinrong Yan [c], Lichao Guo [c], Quanchi Chen [a,*], Xiaobo Zhang [c,*], Huangxian Ju [c]

[a] Division of Spine Surgery Department of Orthopedic Surgery Nanjing Drum Tower Hospital, Affiliated Hospital of Medical School Nanjing University, Nanjing 210008, China
[b] Qingdao Institute for Theoretical and Computational Sciences, Qingdao Institute of Frontier and Interdisciplinary Science, Shandong University, Qingdao 266237, China
[c] State Key Laboratory of Analytical Chemistry for Life Science, School of Chemistry and Chemical Engineering, Nanjing University, Nanjing 210023, China

ARTICLE INFO

Keywords:
Computational speculation
Molecular docking
Single microsphere enrichment
Key protein rapid detection
SARS-CoV-2

ABSTRACT

Detection of key proteins has enormous medical potential, particularly during the initial phase of an outbreak of infectious diseases. For this purpose, we develop a research paradigm based on computational speculation. With the rapid development of computers, it is possible to analyze the structure of key proteins and screen specific fluorescent ligands through computational tools. This process resembles the production of antibodies but is more effective, and the resultant product is significantly cheaper. A proof of concept was demonstrated by studying the S protein of SARS-CoV-2. The structural data of the S protein enabled automated docking with fluorescent molecules. After two rounds of conditional screening and verification, the most effective fluorescent ligand, Protoporphyrin IX (PPIX), was identified. PPIX illuminates the S protein, recovers fluorescence upon binding. The illuminated complex is enriched by a single microsphere, allowing for the quantitative analysis of the proteins through fluorescence intensity. Finally, less than 1000 copies S protein-bearing pseudovirus can be detected in 20 minutes without amplification. Overall, we established a highly sensitive general method for protein detection based on single microsphere enrichment with the aid of computerised simulation. We hope this integrated approach will provide new insights for rapid screening in epidemic populations.

1. Introduction

The coronavirus pandemic has had a profound impact on all aspects of human society [1–3]. From SARS to COVID-19, highly transmissible and pathogenic novel coronavirus has caused a large-scale global health crisis. This makes it more urgent to quickly establish reliable and specific detection methods for frequently mutated virus families [4,5]. At present, the mainstream detection methods are PCR and serological detection methods [6–8]. PCR relies on the results of molecular technology and genome sequencing, and requires experimental verification of a large number of amplification sites [9,10], and complex pretreatment of the sample is required. Antibody detection based immunization methods,such as the most widely used enzyme-linked immunosorbent assay (ELISA) technology, although the sample processing requirements are lower, requires complex biological preparation conditions and a huge workload of antibody screening process [11,12]. Meanwhile, the biologics used in the aforementioned methods are highly dependent on cold-chain transport. The detection method without amplification, because of its compromising sensitivity, usually can't detect viruses within the limits of critical threshold concentrations till the patient has already suffered a serious situation [13]. These shortcomings prevent these methods from being used quickly and on a large scale in the early stages of the pandemic.

Fortunately, In the past decades, computer technology has developed rapidly [14]. With the explosion of computing power, molecular screening can achieve structure-based virtual screening based on very large libraries, and use artificial intelligence (AI) accelerated models and modular screening methods to expedite the acquisition of target molecules [15,16]. For example, structure-based drug design methods can achieve large amounts of data dependent on ligand properties and their 3D structure combined to optimize drug structure, which provides new opportunities for cost-effective small molecule screening [17]. The

* Corresponding authors.
E-mail addresses: DeisenChen@nju.edu.cn (D. Chen), quanchichen@njglyy.com (Q. Chen), xhzxb@nju.edu.cn (X. Zhang).
[1] Yuan Liu, Xiaoyu Xie and Qingyuan Wang contributed equally to this work.

https://doi.org/10.1016/j.snb.2024.136284
Received 21 April 2024; Received in revised form 7 July 2024; Accepted 9 July 2024
Available online 14 July 2024

development of protein structure analysis techniques [18–20] and the computing power of computers have been improved on a large scale. Meanwhile, AI technology has been developed explosively, and relevant proprietary models have been put into practice [21,22]. Against the above background, combining traditional molecular simulations with deep learning makes it cheaper and more efficient to simulate the interactions between different molecules and proteins. This means that the physical and chemical properties of the virus and the mechanism of infection can be analyzed from precise structural data [23,24]. Related studies have revealed the crystal structure of various coronavirus proteins and cell receptor binding domains, including SARS-CoV-2 virus, providing precise target structure information for neutralizing antibodies [25–27]. With the help of AI, thousands of pieces of protein structure information can be turned into parameters that are highly relevant to their function [28]. Because coronavirus spike glycoprotein (S protein) is exposed to the surface and mediates entry into host cells, it is a prime target for neutralizing antibodies during infection [29–32]. It is noteworthy that in every epidemic outbreak caused by multiple sequence mutations, the changes in the structure of the S protein have a certain tendency, and most of its structures are highly conserved [33–35]. This provides a useful research basis for using its sequence information or structural data to predict its target molecules or discover its potential drugs. Thanks to the existing accurate protein structure information and efficient computational tools, we hypothesize that there is a class of small fluorescent molecules similar to antibodies that can bind to target proteins, which can bind to target proteins and act as signaling molecules to directly detect proteins. This scheme circumvents the complexities of biological reagent acquisition, allow for large-scale chemical synthesis and do not require strict storage and transportation conditions. As a proof of concept, we propose a method for screening target small molecules with the help of computational tools, and focus on coronavirus, which causes respiratory infectious diseases, and the key S protein from SARS-CoV-2 was selected for major study [36–41].

Considering the complexity of the S protein detection environment, we propose to use a single microsphere binding aptamer to specifically enrich all targets in the sample to reduce false positive interference due to complex protein environment [42,43]. The microsphere can enable the target objects to be enriched in a very small space on the surface of the microsphere, greatly improving the sensitivity, to meet the standard of clinical detection.

To facilitate subsequent detection, molecules with fluorescent properties were prioritised in this study (Fig. 1A). According to our design concept, the fluorescent molecules required in the experiment exhibit weak or even no fluorescence in their free state. Upon interacting with the target protein, these molecules restore their fluorescence, producing a significant difference in fluorescence intensity compared with their free state, thereby lighting up the protein for quantitative detection. After two rounds of computer-based molecular docking and analysis, a fluorescent ligand protoporphyrin IX (PPIX) was identified. PPIX is an ideal bridge to photosensitization reactions and target-responsive nucleic acid sensors [44], its fluorescence intensity was significantly enhanced after specific binding with the S protein. The final experimental results were in high agreement with the computational speculation conclusions, proving the reliability of the algorithm and providing new insights for related work. The potential fluorescent small molecules can be screened efficiently and quickly. Subsequently, we established a highly sensitive method for the detection of S protein, termed **S**ingle **M**icrosphere **E**nrichment with the aid of **C**omputerised **S**imulation (**SMECS**) (Fig. 1B), a novel approach that combines the superior results of computational simulation screening for the optimal ligand with the powerful enrichment capability of a single microsphere [42,45–47] was developed and achieved high-sensitivity detection of key proteins without amplification (Supplementary material Table S1), proving that SMECS has strong practicality in rapidly establishing diagnostic methods to deal with disease outbreaks.

2. Experimental methods

2.1. Materials and reagents

Thioflavin T (ThT), Zinc phthalocyanine (ZnPc), Thiazole Orange (TO), N-methyl mesoporphyrin IX (NMM), 5,10,15,20-Tetra-(N-methyl-

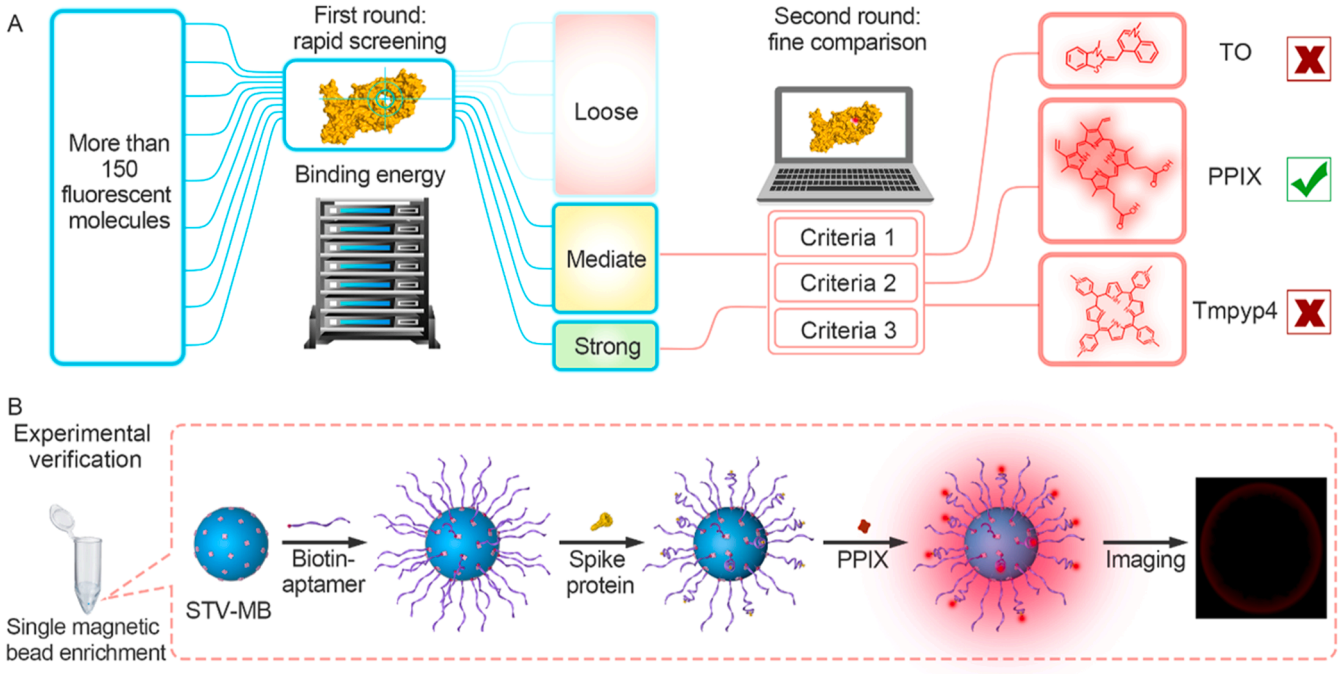

Fig. 1. Schematic Illustration of the Proposed SMECS. (A) A two-round screening mechanism employed to identify fluorescent ligands specific to the key protein (S protein). (B) Schematic representation of S protein detection. The S protein is highly enriched using an SM equipped with S protein aptamers, followed by staining with PPIX obtained from the screening process.

4-pyridyl) porphyrin (TMPyP4) and Protoporphyrin IX (PPIX) were purchased from Thermo Fisher Scientific Inc., USA. The Mag Sepharose microspheres, composed of iron oxide cores embedded in agarose matrices and surface-functionalised with streptavidin (STV-SM), were obtained from Cytiva (Uppsala, SWE). The viral sample collection tubes and oligonucleotide aptamer (5′-Biotin-TTTTTTATCCAGAGTGACG CAGCATCGAGTGGCTTGTTTGTAATGTAGGGTTCCGGTCGTGGGTTG-GACACGGTGGCTTAGT-3′) were acquired from Sangon Biotech, Shanghai, China. The SARS-CoV-2 spike S1+S2 ECD-His recombinant protein (S protein) were purchased from Sino Biological (Shanghai, China). S protein expressed pseudovirus and MERS-CoV were purchased from Vazymes (Nanjing, China). All other chemical reagents were of analytical grade and used as received without further purification.

2.2. Apparatus

The fluorescence spectra were acquired using a FluoroMax-4 spectrofluorophotometer (HITACHI, Japan) and an F980 spectrophotometer (Edinburgh Instruments, UK). Detection images were obtained using an NCF950 NEXCOPE confocal laser scanning microscope (CLSM) (NINGBO YONGXIN OPTICS, China) and an IX71 fluorescence microscope (Olympus, Japan).

2.3. Molecular docking and analysis

AutoDock Vina software [48–50] was utilized in all docking experiments, with the optimised model serving as the docking target. The screening process was confined to molecular docking. To accommodate the universality of the docking range, a larger range parameter encompassing the protein receptor was set for the initial round of binding energy molecular docking. The coordinates for the docking were X: 54.489, Y: −21.837, Z: 22.108, with dimensions X: 110.0 Å, Y: 110.0 Å, Z: 110.0 Å. A higher exhaustiveness, set at 32, was used to achieve relatively high accuracy. Binding affinity result files were exported as LOG files for analysis, and docked structures were visualised to obtain a complete 3D structure of each complex. Details of the first-principle calculation are provided in the Supplementary material online.

2.4. Protein and fluorescent molecular preparation

Considering the mutation process of SARS-CoV-2 [35,51], and the binding mechanism revealed by SARS-CoV-2 RBD related studies [36, 52,53], we selected the typical S protein monomer structure (PDB: 2DD8) after pruning as the receptor model. The.pdb file was imported into AutoDockTools (ADT ver.1.5.6) to prepare a.pdbqt file and create a grid box. Water molecules and other atoms were excluded during this process. The fluorescent molecules screened were primarily derived from the Handbook of Fluorescent Dyes and Probes (R. W. Sabnis, Ph.D., 2015), along with some fluorescent molecules and probes commonly used in this laboratory. Most of the original structural formula files were sourced from PubChem CID (<bold>https://pubchem.ncbi.nlm.nih.gov</bold>). A few were obtained from Chemical Book (<bold>https://www.chemicalbook.com/ProductIndex.aspx</bold>), and the remaining molecules, which were inconvenient to source, were drawn using ChemDraw 2018. All small molecules were optimised using the classical MM2 force field before being submitted to ADT to set the number of torsions and for a.pdbqt file construction.

2.5. Fluorescence spectra of fluorescent ligands bound to S protein

We employed fluorescent ligand binding to the S protein following target enhancement to verify the specific binding effect. The underlying principle is that the fluorescent ligand can specifically bind to a distinct groove site on the S protein, thereby restricting the rotation of the fluorescent molecule and enhancing fluorescence intensity. Fluorescence experiments were conducted using an FS980 fluorescence spectrometer (Edinburgh Technology Ltd, UK) in a quartz cell with a path length of 1 mm. The parameters for the absorption and emission wavelengths of the fluorescent ligands are detailed in Supplementary material Table S2.

2.6. Dissociation constant (K_d) determination

To evaluate the binding affinity between S protein and PPIX, the fluorescence intensity of PPIX with increasing concentrations of S protein were measured. Prior to the measurement, 5 nM PPIX was incubated with 0–10 nM S protein in PBS buffer at 25 °C. Spectra from 550 to 700 nm were collected on FluoroMax-4 spectrofluorophotometer at 25 °C.

The saturation curves for the binding of PPIX with S protein were determined by plotting the fraction of bound PPIX (α, determined by Eq.1) as a function of S protein concentration and fitting with a one-site binding model, using a software of GraphPad Prism 5, to extract the dissociation constant K_d value:

$$\alpha = \frac{F_x - F_0}{F_\infty - F_0} \quad (1)$$

where F_x is the fluorescence intensity at 638 nm for complex of PPIX and DNA with different concentrations, F_∞ and F_0 are the fluorescence intensity in the presence of saturating S protein and in the absence of S protein, respectively. Association constant K_a = [S protein/PPIX]/[S protein][PPIX] is defined as the reciprocal of K_d on the basis of K_a*K_d = 1.

2.7. Preparation and acquisition of SMs

Here, 1 μL of commercial microspheres functionalised with STV were incubated with 0.1 nmol of biotin-aptamer in PBS (10 mM, pH 7.4, containing 137 mM NaCl and 2.7 mM KCl). This mixture was stirred for 1 hour, then washed with PBST (PBS with 0.1 % v/v Tween20) and fixed in 80 μL of PBS. Subsequently, hundreds of microspheres contained in 80 μL of PBS were deposited into a hole in a transparent 96-well plate cover to facilitate the capture of individual microspheres. A micromanipulator system (Narishige) equipped on an Olympus IX53 inverted microscope, complete with a monitor, was used to manipulate an SM. With the assistance of the camera and monitor, we visually identified suitable SMs on the screen. A homemade ruler was employed to select SMs within the desired size range (80 ± 2 μm). Once an appropriate SM was chosen, it was transferred to the tube containing the test sample using a pipette.

2.8. Detection of S protein or pseudovirus particles with SMECS

Here, 1 μL of a series of diluted protein samples or pseudovirus samples in PBS was added to the acquired SM, followed by the addition of 5 μg PPIX into the system. After 20 min of mild stirring at room temperature, each SM was washed with PBST using magnetic separation and then transferred to the microscope for observation.

2.9. Confocal laser scanning microscope imaging for quantitative analysis

The fluorescence images for quantitative analysis were captured using an NCF950 NEXCOPE CLSM. Each SM was placed on a coverslip, and its fluorescence image was obtained by collecting PPIX fluorescence in the TRITC channel of the instrument. The integrated fluorescence intensity of each SM was measured for the quantitative analysis of the target protein or viral particles. It is important to note that the maximum fluorescence value of a bright spot that can be quantitatively acquired by the fluorescence microscope is 225. To capture brighter SM images without exceeding this maximum value, the PMT voltage of the

fluorescence microscope may be adjusted for imaging SMs in different batches under various experimental conditions.

2.10. Fluorescence microscope imaging for quick diagnosis

The fluorescence images for rapid diagnosis were captured using an IX71 fluorescence microscope. Utilising the Cy5 channel. To avoid the photobleaching effect of laser on PPIX, in the process of looking for microspheres in the microscope, we only open the bright field channel, do not open the fluorescence channel. In the bright field channel, the focal plane is adjusted so that the edge of the microsphere is clearest, and the focal plane is the equatorial plane of the microsphere. In the same group of experiments, other detection parameters don't need to be adjusted, only the fluorescence channel should be opened to quickly taking picture. So that the influence of photobleaching can be minimized. Due to the operation of imaging each microsphere is parallel, even if a small amount of photobleaching occurs during the adjustment process, it can ensure that the quenching degree of each sample is the same, and accurate quantification can still be achieved according to the standard curve. It was observed that the microspheres appeared 'illuminated' in the infected group, in contrast to the blank group.

3. Results and discussion

3.1. Fluorescent molecular screening aided by software

We initially used the binding energy values output by AutoDock Vina software for the first round of screening, retaining only those small molecule ligands capable of forming a stable conformation with the S protein. It is crucial to note that each molecule docking with a protein yields a range of binding energies, and for initial screening, we selected the maximum value. To analyse the distribution of the strongest binding energies across all molecules and establish the threshold for actual binding energies, we compiled all binding energy data in Supplementary material Table S3 and illustrated it in Supplementary material Fig. S1. We defined three intervals for evaluation: strong: <-8 kcal/mol; moderate: -7 to -8 kcal/mol; loose: >-7 kcal/mol. Based on the binding energy distribution characteristics in Supplementary material Fig. S1 and the rationale that effective binding should be stronger than hydrogen bonding (typically below -7 kcal/mol) [54], molecules were excluded for the second round of screening. The second round of refined screening was then initiated based on three criteria of conformational analysis. The first criterion was that there should be a region in the protein structure conducive to ligand binding, meaning the predominant (simulated) conformation should primarily associate with this region. Practically, we collected the first nine binding conformations for each molecule based on their binding energy. A molecule was discarded if fewer than four of its conformations were bound to the same protein zone. Following this criterion, only 39 molecules advanced to the next phase (Supplementary material Table S4 and Fig. S2–S4).

The second criterion required the fluorescent molecule bound to the S protein to have a degree of freedom to prevent interference from an overly encapsulating protein structure during energy jumps. Specifically, the simulation condition entailed leaving adequate space at the binding site to ensure that the fluorescent molecule was not completely encapsulated, allowing sufficient contact with the specific site to enhance binding efficiency. Only six molecules met this condition (Supplementary material Table S5 and Fig. S5). Fig. S5 (a-f) indicating target molecules that can be further considered through screening, showed specific binding sites and relatively abundant binding space in their docking results. However, Fig. S5 (g-n) showed some unsatisfactory docking results, such as being completely coated by protein or adsorbed on the protein surface. The final criterion was that candidate molecules should be stable in an aqueous environment (noting that some NHS-esterified fluorescent molecules decompose in water), and their chromophore should remain stable when bound by the S protein. After

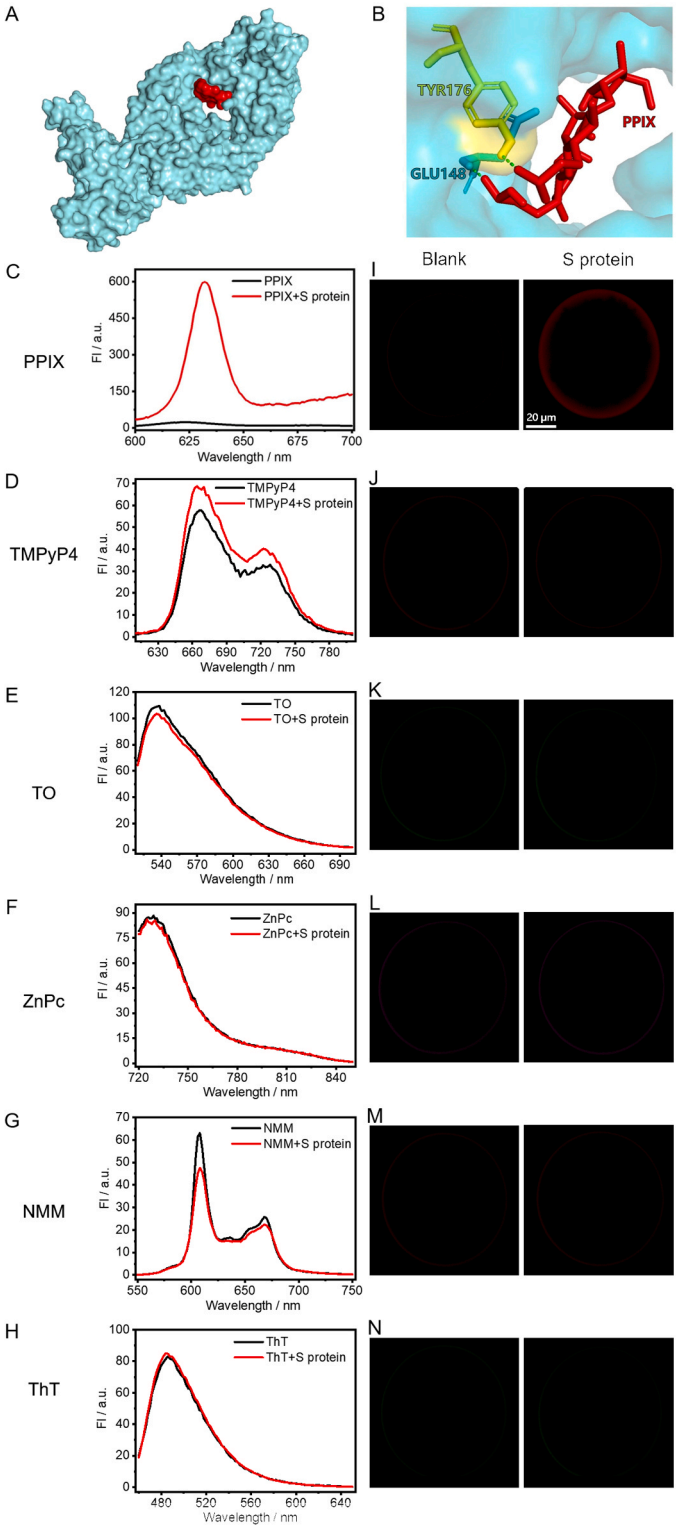

Fig. 2. Binding prediction and validation of different ligands to the S protein. (A) The most dominant binding model of PPIX to the S protein. (B) Analysis of the interaction between PPIX and binding site in the S protein. (C-H) The fluorescence spectra and (I-N) imaging of SM changes after the interaction of TMPyP4, TO, ZnPC, NMM, ThT and PPIX with the S protein. Scale bar: 20 μm.

two rounds of selection, PPIX emerged as the top candidate.

3.2. Binding site prediction and validation

Fig. 2A illustrates the optimal simulated binding between PPIX (in red) and the S protein (in light blue). In the binding region (Fig. 2B), the carboxyl group of PPIX forms two hydrogen bonds (represented by green dotted lines) with adjacent amino acids, ensuring stable attachment of PPIX to this region. Owing to its effective adsorption to S proteins, which are soluble in water, the PPIX-S protein complex exhibits significant fluorescence in an aqueous phase. In contrast, PPIX alone in water does not induce fluorescence due to its extremely low solubility (Fig. 2C). This restoration of fluorescence upon binding with the S protein makes PPIX an ideal candidate for SMECS. Given the relatively limited library of fluorescent molecules and the existence of molecules with similar functions or structures to PPIX in practical applications [55], representative molecules including 5,10,15,20-Tetra-(N-methyl-4 pyridyl) porphyrin (TMPyP4), Thiazole Orange (TO), zinc phthalocyanine (ZnPc), N-methyl mesoporphyrin IX (NMM) and thioflavin T (ThT) were also simulated (Supplementary material Table S6) and experimentally validated (Supplementary material Fig. S6). As shown in the fluorescence spectra (Fig. 2C–H), these molecules exhibit inherent fluorescence in aqueous solutions, but their fluorescence intensity is not significantly enhanced after binding with the S protein. The fluorescence of the complexes formed with S proteins is almost indistinguishable from the molecules alone, rendering them ineffective as high-quality fluorescent ligands for S protein detection. We also enriched the complexes of these molecules with S proteins using SMs for imaging, as illustrated in Fig. 2I–N. Only the PPIX complex with the S protein produced a bright fluorescent image on the microsphere, while the fluorescence images produced by the other molecules post-binding with the S protein were hardly distinguishable from the blank sample. Except for PPIX, no other molecule met the above criteria, nor did they exhibit solubility enhancement in the aqueous phase with the aid of S protein (Supplementary material Table S6 and Fig. S6), reaffirming considerable advantage of PPIX. To evaluate the binding affinity between PPIX and S protein, we conduct experiment to measure the K_d value of PPIX against S protein (Supplementary material Fig. S7). According to the experimental results, K_d is calculated to be 9.5 nM, the ideal K_d guarantees the application of this computational simulation to S protein high sensitivity detection.

After identifying PPIX as the detection ligand for the S protein, S proteins of other variants of SARS-COV-2 (Alpha PDB ID:7NEH, Beta PDB ID:7S5P, Delta PDB ID:7W9F, Omicron PDB ID:7QNW) were also performed docking with mentioned fluorescent molecular (Supplementary material Table. S7). Similar to the previous results, in the Table. S7 we can see that TMPyP4, TO, ZnPc, NMM and ThT are also unqualified ligands that does not conform to cri1 or/and cri2. While PPIX still shows a very good docking with their S protein. The experimental results show that our method has certain tolerance for the protein structure after virus mutation and can be quickly applied to the detection of viral proteins of the same family. In addition, predicting the specificity of the detection method through computational simulation is also an important basis for the method to be put into practical application. We also simulated PPIX as a ligand docking with S proteins of other coronaviruses causing respiratory disease and certain proteins in throat swabs that have potential interfere with the accuracy of the experiment (Supplementary material Table. S8 and Fig. S8). In these simulation results, we can see those coronaviruses, such as bat (PDB ID:5XGR) coronaviruses, HKU1 (PDB ID:5KWB) coronaviruses, MERS_S (PDB ID:7C02) coronaviruses, can't docking with PPIX perfect. The docking results of PPIX docking with common endogenous interfering substances in throat swab, such as HAMA (PDB ID:2Z4Q), lysozyme (PDB ID:168 L), Nucleocapsid (PDB ID:6WZO), RF_IgG (PDB ID:1ADQ), are also very unsatisfactory. These simulation results provide a basis for the specificity of the experimental detection, and we will verify these results in the subsequent specificity analysis of the experiment.

3.3. High-sensitivity S protein detection

Next, we optimized the parameters of the experiment (Supplementary material Fig. S9) and then conducted highly sensitive detection of the S protein by combining PPIX with the enrichment system, wherein aptamers on SM target the S protein specifically. To precisely demonstrate the detection capability of the system, we utilised a CLSM system to image the equatorial plane of these SMs. This approach was chosen because the edges of the SMs appear clearest in the bright field, thereby minimising errors associated with focusing. Since the samples are bound to the surface of the microsphere, signals of each system will appear as an aureole.

Fig. 3 illustrates the results of the 100–5000 pg/mL S protein assay compared with a blank. One of the three parallel groups imaging results (Supplementary material Fig. S10) of SMs were disposed in Fig. 3A. The top panel in Fig. 3A displays both bright field and fluorescence images of SMs detecting various concentrations of S protein. The bottom panel presents pseudo-colour bars and quantitative fluorescence images processed using the pseudo-colour method. As shown in Fig. 3A, the fluorescence intensity of the SMs increases with higher S protein concentrations. In addition, the pseudo-colour processed images at different S protein concentrations are easily distinguishable by the naked eye, enabling rapid semi-quantitative analysis. Fig. 3B depicts the detection curve for the S protein. The quantitative results were obtained by integrating the fluorescence intensities (FI) from each pixel in the SM images. The integrated FI of the SMs are linearly proportional to the logarithm of the S protein concentrations, ranging from 100 pg/mL to 5000 pg/mL. The correlation equation is $FI = 4.86 \times 10^5 \lg C_{s\ protein}$ (pg/mL) - 9.52×10^5, with a correlation coefficient (R) of 0.9961. The limit of detection was calculated to be 95.56 pg/mL (1.24 pM).

We also mixed PPIX with S protein in a homogeneous solution and quantified S protein by detecting the fluorescence intensity of the solution, so that only 10 ng/mL of S protein could be detected (Supplementary material Fig. S11). For protein detection, the SM-based target enrichment method is highly sensitive, even without signal amplification. In addition, computer simulations can assist in rapidly screening out optimal signal molecules by analysing the structures of proteins and ligands at the onset of infectious disease outbreaks, thus achieving high-sensitivity detection. As indicated in Table S1, the limit of detection using common immunoassay is typically at the nM level. Thanks to limited by antibody culture and experimental screening, earlier detection methods became available more than four months after the outbreak of the epidemic, limiting their effectiveness during critical periods. In contrast, our method, which employs ready-made small molecule ligands, circumvents these issues. It combines computer simulation with target enrichment by SM, facilitating the rapid development of high-sensitivity detection methods in the early stages of outbreaks.

3.4. Specificity of the SMECS for S protein detection

Detecting the concentration of S protein in complex real samples accurately, the specificity of the detection method is crucial. To determine whether human proteins in throat swab samples or other coronaviruses influence the detection of S protein using SMECS, we conducted experiments replacing the S protein standard samples with some endogenous interfering proteins in throat swabs, S protein of other coronavirus-like viruses and negative throat swab samples. Fig. 4 displays the results of the fluorescence imaging. Fig. 4A shows that the

brightness of the SMs detecting the negative throat swab sample and other proteins except the S protein is very weak, making them indistinguishable from the blank control. In contrast, the SM-detecting S protein exhibits strong fluorescence intensity. Fig. 4B shows a histogram representing the relative fluorescence response values of different

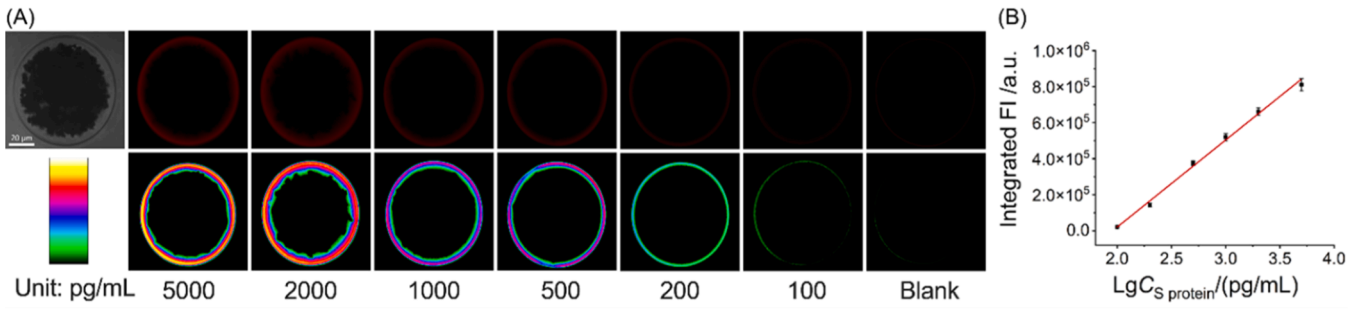

Fig. 3. S protein quantitative detection results. (A) The top panel reveals bright field and fluorescence images of SMs detecting a series of S protein concentrations; the bottom panel shows a pseudo-colour bar and fluorescence images treated with the pseudo-colour method. (Settings for imagining: HV of PMT: 40, laser power of a 561 nm laser: 20. The scale bar: 20 μm.). (B) A Linear fit curve for the integrated fluorescence intensities (FI) of the SM and S protein concentrations. Error bars represent the standard deviation from three independent measurements.

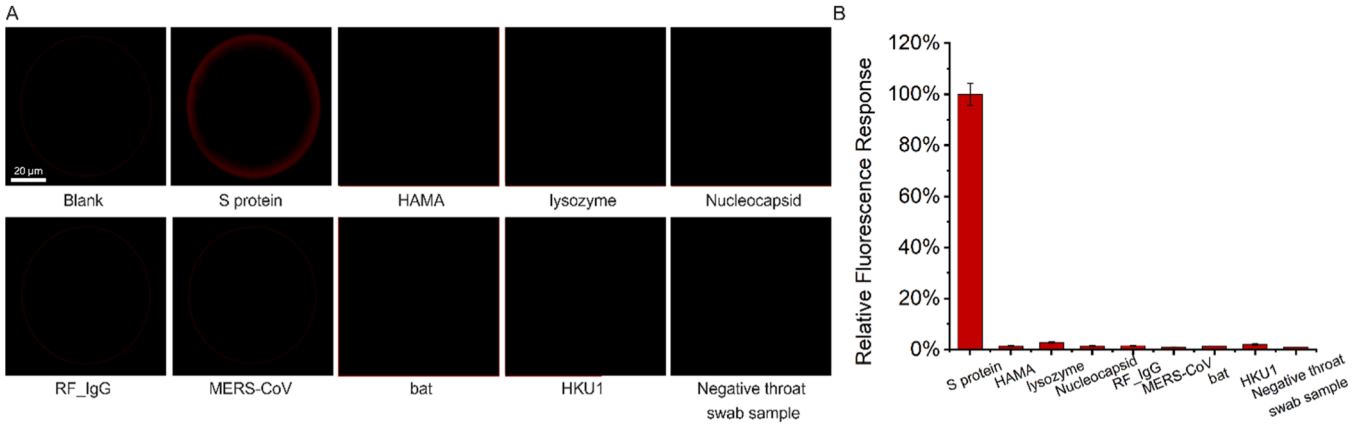

Fig. 4. Specificity evaluation of the high-sensitivity S protein detection. (A) Fluorescence images of SMs detecting a blank, the S protein, some endogenous interfering proteins in throat swabs, S protein of other coronavirus-like viruses and negative throat swab samples interacting with PPIX, all under identical experimental conditions. (HV of PMT for the imaging: 40, laser power of 561 nm laser: 20. The scale bar: 20 μm.) (B) A histogram for the relative integrated fluorescence intensity of each SM detecting different samples; error bars represent the standard deviation from three independent measurements.

samples, calculated by integrating the fluorescence intensity and subtracting the blank value. Notably, the interference from proteins in throat swab samples and other coronaviruses on S protein detection is minimal, confirming the high specificity of our method for detecting S protein. This also further verifies the feasibility of our molecular screening scheme, providing a reliable reference for the rapid development of detection methods during the early stages of an epidemic.

3.5. *Quantification of SARS-CoV-2 in real throat swab samples with SMECS*

To confirm the ability of our analytical method to detect SARS-CoV-2 by targeting the S protein, we tested actual virus samples. Throat swabs from healthy volunteers served as negative controls, while pseudoviruses were added to create positive samples. The experimental results are displayed in Fig. 5. As depicted in Fig. 5A, a single SARS-CoV-2 typically harbours hundreds of S proteins trimer [56], leading to signal amplification when the targets are changed to SARS-CoV-2, thereby enhancing the sensitivity of the method for virus detection. Fig. 5B demonstrates that samples with as few as 720 viruses can still produce a fluorescence signal on the microsphere, distinctly different from the negative sample. Considering the widespread availability of general fluorescence microscopy in frontline settings, Fig. 5C shows the corresponding results from standard fluorescence microscopy. Since each SM possesses a varying percentage of magnetic centres differences in the thickness of the outer transparent layer can influence the imaging results. In contrast, the light cut-off layer utilised in confocal microscopy

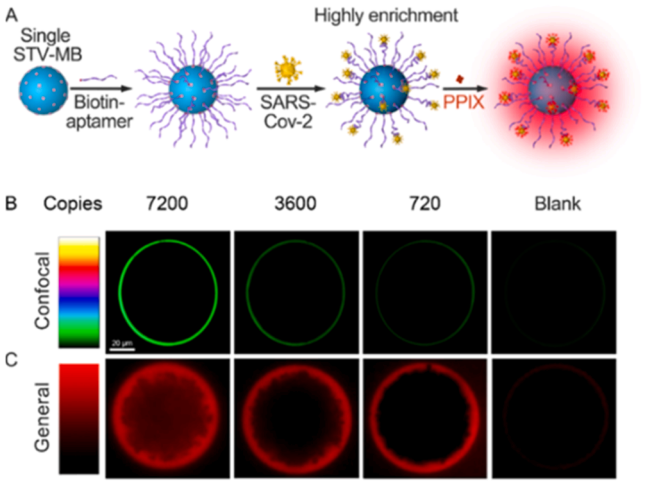

Fig. 5. Schematic diagram and detection results of actual samples. (A) Schematic diagram of SARS-CoV-2 detection with SM capturing the S protein. The primary difference from the previously mentioned detection method is that the target is SARS-CoV-2 instead. (B) The results from confocal imaging at low viral content. (C) The corresponding results were obtained using normal fluorescence microscopy imaging. Scale bar: 20 μm.

avoids interference from outside the non-focal plane, making its imaging results suitable for quantitative analysis. Although the imaging results are not as precise as those from confocal microscopy, it is encouraging that low concentrations of pseudoviruses can be effectively distinguished under general microscopy.

4. Conclusions

In this study, we proposed an efficient method, SMECS, for screening fluorescent small molecule ligands based on protein structure for key proteins and their carrier detection. SMECS comprises two core technologies: computational speculation and an SM enrichment strategy. Based on precise protein structures, the computer identifies fluorescent ligands that specifically bind to the target protein in a vast molecular library. Notably, the two-round screening algorithm detailed in this paper has been instrumental in studying S proteins, identifying PPIX as the fluorescent ligand. PPIX, a small molecule compound, is advantageous because of its large-scale availability, ease of storage and low cost. This represents a significant improvement over the biological preparation of antibodies required for ELISA and other immune methods, enabling the rapid establishment of detection methods at the onset of large-scale epidemic outbreaks, which is crucial in practical medical scenarios. Furthermore, we employed the SM enrichment technique for high-sensitivity detection of the target protein without amplification. In our demonstrations using the SARS-CoV-2-associated S protein, the pre-screened fluorescent ligand PPIX efficiently stains highly enriched S proteins or their carriers, enabling user-friendly detection via standard fluorescence microscopy. We anticipate that the research approaches detailed in this paper will pave the way for the future development and practical application of rapid and ultra-sensitive detection methods for other proteins. At the same time, it is also hoped to establish a small and convenient fluorescence analysis platform to meet the daily detection needs of the community.

CRediT authorship contribution statement

Quanchi Chen: Writing – original draft, Resources, Project administration, Methodology, Funding acquisition, Conceptualization. **Xiaobo Zhang:** Writing – review & editing, Writing – original draft, Resources, Methodology, Formal analysis, Data curation, Conceptualization. **Xinrong Yan:** Visualization, Validation, Supervision, Methodology, Conceptualization. **Lichao Guo:** Visualization, Methodology, Funding acquisition, Formal analysis, Conceptualization. **Desheng Chen:** Writing – review & editing, Writing – original draft, Methodology, Investigation, Data curation, Conceptualization. **Dehui Qiu:** Supervision, Resources, Project administration, Conceptualization. **Xiaoyu Xie:** Writing – original draft, Software, Resources, Data curation, Conceptualization. **Qingyuan Wang:** Visualization, Investigation, Funding acquisition, Conceptualization. **Yuan Liu:** Validation, Supervision, Software, Formal analysis, Data curation, Conceptualization. **Huangxian Ju:** Writing – original draft, Resources, Conceptualization.

Declaration of Competing Interest

We declare that we do not have any commercial or associative interest that represents a conflict of interest in connection with the work submitted.

Data availability

The data that has been used is confidential.

Acknowledgement

We gratefully acknowledge the financial support from the National Natural Science Foundation of China (22004062, 82102637, 21890741 and 21827812), China Postdoctoral Science Foundation (2021M701675), Key Laboratory of Analytical Chemistry for Life Science (SKLACLS2109) and Key Laboratory of Applied Surface and Colloid Chemistry (Shaanxi Normal University).

Appendix A. Supporting information

Supplementary data associated with this article can be found in the online version at doi:10.1016/j.snb.2024.136284.

References

[1] M. Chan-Yeung, R.H. Xu, SARS: epidemiology, Respirology 8 (2003) S9–S14.
[2] M. Nicola, Z. Alsafi, C. Sohrabi, A. Kerwan, A. Al-Jabir, C. Iosifidis, et al., The socio-economic implications of the coronavirus pandemic (COVID-19): a review, Int. J. Surg. 78 (2020) 185–193.
[3] H. Wang, K.R. Paulson, S.A. Pease, S. Watson, H. Comfort, P. Zheng, et al., Estimating excess mortality due to the COVID-19 pandemic: a systematic analysis of COVID-19-related mortality, 2020–21, Lancet 399 (2022) 1513–1536.
[4] P.A. Rota, M.S. Oberste, S.S. Monroe, W.A. Nix, R. Campagnoli, J.P. Icenogle, et al., Characterization of a novel coronavirus associated with severe acute respiratory syndrome, Science 300 (2003) 1394–1399.
[5] B. Udugama, P. Kadhiresan, H.N. Kozlowski, A. Malekjahani, M. Osborne, V.Y. C. Li, et al., Diagnosing COVID-19: the disease and tools for detection, ACS Nano 14 (2020) 3822–3835.
[6] H. Hempel, M. Page, T. Kemp, A. Semper, T. Brooks, L.A. Pinto, The importance of using WHO International Standards to harmonise SARS-CoV-2 serological assays, Lancet Microbe 5 (2024) e301–e305.
[7] C. Huang, Y. Wang, X. Li, L. Ren, J. Zhao, Y. Hu, et al., Clinical features of patients infected with 2019 novel coronavirus in Wuhan, China, Lancet 395 (2020) 497–506.
[8] K. Manten, S. Katzenschlager, L.E. Brümmer, S. Schmitz, M. Gaeddert, C. Erdmann, et al., Clinical accuracy of instrument-based SARS-CoV-2 antigen diagnostic tests: a systematic review and meta-analysis, Viro. J. 21 (2024) 99.
[9] B. Hu, H. Guo, P. Zhou, Z.-L. Shi, Characteristics of SARS-CoV-2 and COVID-19, Nat. Rev. Microbiol. 19 (2020) 141–154.
[10] T. Li, Diagnosis and clinical management of severe acute respiratory syndrome Coronavirus 2 (SARS-CoV-2) infection: an operational recommendation of Peking Union Medical College Hospital (V2.0), Emerg. Microbes Infect. 9 (2020) 582–585.
[11] Y. Chen, F. Liu, L.P. Lee, Quantitative and ultrasensitive in situ immunoassay technology for SARS-CoV-2 detection in saliva, Sci. Adv. 8 (2022) eabn3481.
[12] J. Liu, G. Ruan, W. Ma, Y. Sun, H. Yu, Z. Xu, et al., Horseradish peroxidase-triggered direct in situ fluorescent immunoassay platform for sensing cardiac troponin I and SARS-CoV-2 nucleocapsid protein in serum, Biosens. Bioelectron. 198 (2022) 113823.
[13] L. Guo, L. Ren, S. Yang, M. Xiao, D. Chang, F. Yang, et al., Profiling early humoral response to diagnose novel coronavirus disease (COVID-19), Clin. Infect. Dis. 71 (2020) 778–785.
[14] M. Pandey, M. Fernandez, F. Gentile, O. Isayev, A. Tropsha, A.C. Stern, A. Cherkasov, The transformational role of GPU computing and deep learning in drug discovery, Nat. Mach. Intell. 4 (2022) 211–221.
[15] A.V. Sadybekov, V. Katritch, Computational approaches streamlining drug discovery, Nature 616 (2023) 673–685.
[16] A. Zhavoronkov, Y.A. Ivanenkov, A. Aliper, M.S. Veselov, V.A. Aladinskiy, A. V. Aladinskaya, et al., Deep learning enables rapid identification of potent DDR1 kinase inhibitors, Nat. Biotechnol. 37 (2019) 1038–1040.
[17] T. Talele, S. Khedkar, A. Rigby, Successful applications of computer aided drug discovery: moving drugs from concept to the clinic, Curr. Top. Med. Chem. 10 (2010) 127–141.
[18] J. Chen, R. Wang, N.B. Gilby, G.-W. Wei, Omicron variant (B.1.1.529): infectivity, vaccine breakthrough, and antibody resistance, J. Chem. Inf. Model. 62 (2022) 412–422.
[19] D. Wrapp, N. Wang, K.S. Corbett, J.A. Goldsmith, C.-L. Hsieh, O. Abiona, et al., Cryo-EM structure of the 2019-nCoV spike in the prefusion conformation, Science 367 (2020) 1260–1263.
[20] R. Yan, Y. Zhang, Y. Li, L. Xia, Y. Guo, Q. Zhou, Structural basis for the recognition of SARS-CoV-2 by full-length human ACE2, Science 367 (2020) 1444–1448.
[21] D.E. Graff, E.I. Shakhnovich, C.W. Coley, Accelerating high-throughput virtual screening through molecular pool-based active learning, Chem. Sci. 12 (2021) 7866–7881.
[22] P. Schneider, W.P. Walters, A.T. Plowright, N. Sieroka, J. Listgarten, R. A. Goodnow, et al., Rethinking drug design in the artificial intelligence era, Nat. Rev. Drug Discov. 19 (2019) 353–364.
[23] A.A. Sadybekov, A.V. Sadybekov, Y. Liu, C. Iliopoulos-Tsoutsouvas, X.-P. Huang, J. Pickett, et al., Synthon-based ligand discovery in virtual libraries of over 11 billion compounds, Nature 601 (2021) 452–459.
[24] X. Yang, Y. Wang, R. Byrne, G. Schneider, S. Yang, Concepts of artificial intelligence for computer-assisted drug discovery, Chem. Rev. 119 (2019) 10520–10594.
[25] A.C. Walls, Y.-J. Park, M.A. Tortorici, A. Wall, A.T. McGuire, D. Veesler, Structure, function, and antigenicity of the SARS-CoV-2 spike glycoprotein, Cell 181 (2020) 281–292, e6.

[26] W. Wu, Y. Cheng, H. Zhou, C. Sun, S. Zhang, The SARS-CoV-2 nucleocapsid protein: its role in the viral life cycle, structure and functions, and use as a potential target in the development of vaccines and diagnostics, Virol. J. 20 (2023) 6.
[27] J. Zhang, A. Ejikemeuwa, V. Gerzanich, M. Nasr, Q. Tang, J.M. Simard, R.Y. Zhao, Understanding the role of SARS-CoV-2 ORF3a in viral pathogenesis and COVID-19, Front. Microbiol. 13 (2022).
[28] C. Wu, Y. Liu, Y. Yang, P. Zhang, W. Zhong, Y. Wang, et al., Analysis of therapeutic targets for SARS-CoV-2 and discovery of potential drugs by computational methods, Acta Pharm. Sin. B. 10 (2020) 766–788.
[29] S.F. Ahmed, A.A. Quadeer, M.R. McKay, Preliminary identification of potential vaccine targets for the COVID-19 coronavirus (SARS-CoV-2) based on SARS-CoV immunological studies, Viruses 12 (2020) 254.
[30] A.M. Carabelli, T.P. Peacock, L.G. Thorne, W.T. Harvey, J. Hughes, T.I. de Silva, et al., SARS-CoV-2 variant biology: immune escape, transmission and fitness, Nat. Rev. Microbiol. 21 (2023) 162–177.
[31] J. Lan, J. Ge, J. Yu, S. Shan, H. Zhou, S. Fan, et al., Structure of the SARS-CoV-2 spike receptor-binding domain bound to the ACE2 receptor, Nature 581 (2020) 215–220.
[32] Y. Watanabe, J.D. Allen, D. Wrapp, J.S. McLellan, M. Crispin, Site-specific glycan analysis of the SARS-CoV-2 spike, Science 369 (2020) 330–333.
[33] H.M. Ashour, W.F. Elkhatib, M.M. Rahman, H.A. Elshabrawy, Insights into the recent 2019 novel coronavirus (SARS-CoV-2) in light of past human coronavirus outbreaks, Pathogens 9 (2020) 186.
[34] Mm.M. Hatmal, W. Alshaer, M.A.I. Al-Hatamleh, M. Hatmal, O. Smadi, M.O. Taha, et al., Comprehensive structural and molecular comparison of spike proteins of SARS-CoV-2, SARS-CoV and MERS-CoV, and their interactions with ACE2, Cells 9 (2020) 2638.
[35] A. Wu, L. Wang, H.Y. Zhou, C.Y. Ji, S.Z. Xia, Y. Cao, et al., One year of SARS-CoV-2 evolution, Cell Host Microbe 29 (2021) 503–507.
[36] C. Bai, J. Wang, G. Chen, H. Zhang, K. An, P. Xu, et al., Predicting mutational effects on receptor binding of the spike protein of SARS-CoV-2 variants, J. Am. Chem. Soc. 143 (2021) 17646–17654.
[37] S.M. Gobeil, K. Janowska, S. McDowell, K. Mansouri, R. Parks, V. Stalls, et al., Effect of natural mutations of SARS-CoV-2 on spike structure, conformation, and antigenicity, Science 373 (6555) (2021).
[38] R. Khan, A.S. Deshpande, G. Proteasa, S. Andreescu, Aptamer-based electrochemical biosensor with S protein binding affinity for COVID-19 detection: integrating computational design with experimental validation of S protein binding affinity, Sens. Actuat. B Chem. 399 (2024) 134775.
[39] J. Lan, J. Ge, J. Yu, S. Shan, H. Zhou, S. Fan, et al., Structure of the SARS-CoV-2 spike receptor-binding domain bound to the ACE2 receptor, Nature 581 (2020) 215–220.
[40] J. Singh, S. Vashishtha, B. Kundu, Spike protein mutation-induced changes in the kinetic and thermodynamic behavior of its receptor binding domains explain their higher propensity to attain open states in SARS-CoV-2 variants of concern, ACS Cent. Sci. 9 (2023) 1894–1904.
[41] A.C. Walls, Y.J. Park, M.A. Tortorici, A. Wall, A.T. McGuire, D. Veesler, Structure, function, and antigenicity of the SARS-CoV-2 spike glycoprotein, Cell 181 (2020) 281–292, e6.
[42] D. Chen, X. Zhang, L. Zhu, C. Liu, Z. Li, All on size-coded single bead set: a modular enrich-amplify-amplify strategy for attomolar level multi-immunoassay, Chem. Sci. 13 (2022) 3501–3506.
[43] X. Liu, Y.L. Wang, J. Wu, J. Qi, Z. Zeng, Q. Wan, et al., Neutralizing aptamers block s/rbd-ace2 interactions and prevent host cell infection, Angew. Chem. Int. Ed. Engl. 60 (2021) 10273–10278.
[44] Y. Lin, X. Chen, Y. Li, Y. Ye, L. Yang, L. Liao, et al., Scandium-mediated photosensitization oxidation: a new strategy for fast and neutral pH colorimetric detection of cocaine by coupling split aptamer, Sens. Actuat. B Chem. 380 (2023) 133349.
[45] D. Chen, X. Zhang, L. Zhu, C. Liu, Z. Li, Single microbead-anchored fluorescent immunoassay (SMFIA): a facile and versatile platform allowing simultaneous detection of multiple antigens, Chem. Asian J. 12 (2017) 2894–2898.
[46] X. Zhang, C. Liu, L. Sun, X. Duan, Z. Li, Lab on a single microbead: an ultrasensitive detection strategy enabling microRNA analysis at the single-molecule level, Chem. Sci. 6 (2015) 6213–6218.
[47] X. Zhang, C. Liu, H. Wang, H. Wang, Z. Li, Rare earth ion mediated fluorescence accumulation on a single microbead: an ultrasensitive strategy for the detection of protein kinase activity at the single-cell level, Angew. Chem. Int. Ed. Engl. 54 (2015) 15186–15190.
[48] J. Eberhardt, D. Santos-Martins, A.F. Tillack, S. Forli, AutoDock Vina 1.2.0: new docking methods, expanded force field, and python bindings, J. Chem. Inf. Model. 61 (2021) 3891–3898.
[49] O. Trott, A.J. Olson, AutoDock Vina: improving the speed and accuracy of docking with a new scoring function, efficient optimization, and multithreading, J. Comput. Chem. 31 (2010) 455–461.
[50] Z. Wang, H. Sun, X. Yao, D. Li, L. Xu, Y. Li, et al., Comprehensive evaluation of ten docking programs on a diverse set of protein-ligand complexes: the prediction accuracy of sampling power and scoring power, Phys. Chem. Chem. Phys. 18 (2016) 12964–12975.
[51] H. Yao, Y. Song, Y. Chen, N. Wu, J. Xu, C. Sun, et al., Molecular architecture of the SARS-CoV-2 virus, Cell 183 (2020) 730–738, e13.
[52] Y. Dong, T. Dai, J. Liu, L. Zhang, F. Zhou, Coronavirus in continuous flux: from SARS-CoV to SARS-CoV-2, Adv. Sci. 7 (2020) 2001474.
[53] P. Prabakaran, J. Gan, Y. Feng, Z. Zhu, V. Choudhry, X. Xiao, et al., Structure of severe acute respiratory syndrome coronavirus receptor-binding domain complexed with neutralizing antibody, J. Biol. Chem. 281 (2006) 15829–15836.
[54] N.N. Greenwood, A. Earnshaw, Chemistry of the Elements, Elsevier Science, 2012.
[55] J.L. Mergny, D. Sen, DNA quadruple helices in nanotechnology, Chem. Rev. 119 (2019) 6290–6325.
[56] Y.M. Bar-On, A. Flamholz, R. Phillips, R. Milo, SARS-CoV-2 (COVID-19) by the numbers, elife 9 (2020).

Yuan Liu received his B.Sci. degree in chemistry from Hebei University China. Currently, he is doing researches about biosensing.

Xiaoyu Xie received his PhD. from Nanjing University. He is working in Shandong University, and his current research focuses on computational chemistry related fields.

Qingyuan Wang received his PhD. from Nanjing Medical University. He is working in Nanjing Drum Tower Hospital (The Affiliated Hospital of Medical School Nanjing), and his current research focuses on cancer treatment related fields.

Desheng Chen received his Ph.D. degrees from University of Science and Technology Beijing. He is working in Nanjing University, and his current research focuses on life analytical sciences related fields.

Dehui Qiu is currently a graduate student for his Ph.D. degree in Nanjing University focusing on chemical catalysis related fields.

Xinrong Yan is currently a graduate student for his Ph.D. degree in Nanjing University focusing on analytical chemistry related fields.

Lichao Guo received his B.Sci. degree in chemistry from Hebei University China. Currently, he is doing his Master's degree in related fields of organic synthesis.

Quanchi Chen received his PhD. from Leiden University. He is working in Division of Spine Surgery Department of Orthopedic Surgery Nanjing Drum Tower Hospital, Affiliated Hospital of Medical School Nanjing University Nanjing.

Xiaobo Zhang received his Ph.D. degrees from Nanjing University. He is working in Nanjing University, and his current research focuses on life analytical chemistry fields.

Huangxian Ju In 1986, 1989 and 1992, received his bachelor of Science degree, master's degree and doctor's degree from Nanjing University respectively. He was a professor at Nanjing University in 1999. His main research fields include immunoassay, cell analytical chemistry, nanobiosensing, bioimaging and clinical molecular diagnosis.